Structural Study of δ-AlOOH Up to 29 GPa

Dariia Simonova [1], Elena Bykova [2], Maxim Bykov [1,2], Takaaki Kawazoe [3], Arkadiy Simonov [4], Natalia Dubrovinskaia [5] and Leonid Dubrovinsky [1,*]

[1] Bavarian Research Institute of Experimental Geochemistry and Geophysics, University of Bayreuth, D-95440 Bayreuth, Germany; dariia.simonova@gmail.com (D.S.); maks.byk@gmail.com (M.B.)

[2] Earth and Planets Laboratory, Carnegie Institution for Science, Washington, DC 20015, USA; ebykova@carnegiescience.edu

[3] Department of Earth and Planetary Systems Science, Hiroshima University, Higashi-Hiroshima 739-8526, Japan; kawazoe@hiroshima-u.ac.jp

[4] Laboratory for Multifunctional Ferroic Materials, Materials Department, ETH Zürich, 8093 Zürich, Switzerland; arkadiy.simonov@mat.ethz.ch

[5] Laboratory of Crystallography, University of Bayreuth, D-95440 Bayreuth, Germany; natalia.dubrovinskaia@uni-bayreuth.de

* Correspondence: leonid.dubrovinsky@uni-bayreuth.de

Abstract: A structure and equation of the state of δ-AlOOH has been studied at room temperature, up to 29.35 GPa, by means of single crystal X-ray diffraction in a diamond anvil cell using synchrotron radiation. Above ~10 GPa, we observed a phase transition with symmetry changes from $P2_1nm$ to $Pnnm$. Pressure-volume data were fitted with the second order Birch-Murnaghan equation of state and showed that, at the phase transition, the bulk modulus (K_0) of the calculated wrt 0 pressure increases from 142(5) to 216(5) GPa.

Keywords: AlOOH; diamond anvil cell; high pressure; extreme conditions; single crystal X-ray diffraction (SC-XRD)

1. Introduction

Water and water-bearing minerals are important components in the Earth crust and mantle. For many years, the whole mantle and especially the lower mantle was thought to be anhydrous, particularly since most of the known hydrous phases lose water with the increasing temperature even at high pressure. However, there is solid evidence available now that some of the H-bearing phases survive even at lower mantle conditions [1,2]. If water is transported into the deep mantle and released there, the elasticity, viscosity, melting temperature, and atomic diffusion properties of the mantle constituents would be considerably affected. Therefore, the properties of high-pressure hydrous minerals play an important role for understanding the petrology and geochemical evolution of the Earth.

The obvious possible sources of water in the lower mantle are thought to be hydrated magnesium and aluminum silicates, i.e., phases within the (MgO/Al_2O_3)-SiO_2-H_2O systems. The aluminous hydrous silicate, the phase Egg ($AlSiO_3(OH)$), was found in inclusions of natural diamonds [3], proving that this mineral is present in deep Earth interiors. At the same time, high-pressure and high-temperature experiments document that the phase Egg is formed in the hydrous sediment component in the upper mantle [4]. In addition, it decomposes with the formation of δ-AlOOH and stishovite at the base of the mantle transition zone [5,6], which makes δ-AlOOH a prominent candidate phase for the water transport in the lower mantle conditions [7]. This attracted a lot of attention and

currently the structure of δ-AlOOH [8–12], its stability range [6,13–17], and physical properties [18,19] have been investigated both theoretically and experimentally.

The δ-AlOOH phase is a high-pressure polymorph of the natural aluminous hydrous minerals diaspore (α-AlOOH) and boehmite (γ-AlOOH) [10,20]. At ambient conditions, δ-AlOOH can be obtained as a metastable phase with the orthorhombic symmetry with space group $P2_1nm$ [20,21]. In this structure, an aluminum atom is surrounded by six oxygen atoms forming a distorted octahedral coordination. These AlO_6 octahedra share edges to form an infinite chain along the a axis of the orthorhombic unit cell (Figure 1a). At ambient conditions, the Al atom is displaced from the center of the octahedra to compensate for the electrostatic charge difference caused by hydrogen bonds.
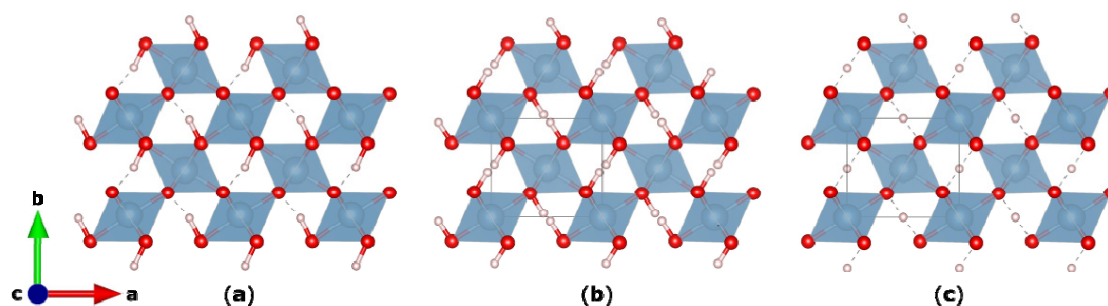
Figure 1. Crystal structure of δ-AlOOH shown in the projection along the *c* direction at the ambient pressure space group $P2_1nm$ (**a**) and at the high symmetry phase *Pnnm*, featuring disordered hydrogen in the intermediate phase between 9 and 18 GPa (**b**) and symmetric hydrogen above 18 GPa (**c**).

At a pressure approximately above 9 GPa, the δ-AlOOH goes through a phase transition which increases the symmetry from $P2_1nm$ to *Pnnm* [11]. The new symmetry elements include the 2-fold axis passing through the middle of the hydrogen bond and making the AlO_6 tetrahedra more symmetric. Structural studies found no jump in the unit cell parameters at the phase transition. However, the crystal becomes much stiffer, especially along the **a** and **b** axes, which coincide with the direction of the hydrogen bond. The mechanism of this stiffening is interesting since, as was recently shown by the neutron study [12], the phase transition does not correspond to symmetrization of the hydrogen bond (i.e., formation of the stiff hydrogen bond where hydrogen occupies the position in the center between two oxygen atoms). Rather, at the phase transition, hydrogen becomes disordered (Figure 1), while the symmetrization of the hydrogen bond happens only above 18 GPa and, intriguingly, is not associated with the unit cell stiffening [12].

Understanding this unusual behavior would require accurate ab-initio modelling, which so far has been proven complicated. Ordered models at absolute zero temperature predict hydrogen symmetrization at a very high pressure of about 30 GPa [18], while completely missing the order-disorder phase transition. High-temperature DFT-MD simulations show the order-disorder phase transition [22], but the small supercell size used so far could not provide reliable estimates of material stiffness and the phase transition pressure. An accurate model will require very large supercells and potentially a careful modelling of hydrogen tunneling to capture the disorder driven stiffening. In addition, it will require accurate experimental reference structures, which we aim to provide in this study. Moreover, there is inconsistency in the reported compressibility of δ-AlOOH with the bulk modulus (in GPa)/first derivatives ranging from 228/7 [13] to 124/13.5 [9], which require additional investigations.

In this work, we report the results of a single crystal experiment on δ-AlOOH at pressures up to about 30 GPa, using the diamond anvil cell (DAC) technique. In addition, we determined its lattice parameters and revealed the crystal structure by means of X-ray diffraction at a synchrotron facility. To the best of our knowledge, this is the first work in which the structure of δ-AlOOH was investigated, using single crystal diffraction above 12 GPa.

2. Materials and Methods

Single crystals of δ-AlOOH were synthesized at high-pressure and high-temperature conditions at Bayerisches Geoinstitut (Bayreuth, Germany). The synthesis was performed by decomposition of $Al(OH)_3$ at 21 GPa and 1050 °C upon heating during 4 h in a 1000 ton multi-anvil Haymag press.

High-quality single crystals with an average size of ~0.02 × 0.02 × 0.03 mm^3 were preselected and the data collection was performed at ambient conditions, using a three-circle diffractometer equipped with a SMART APEX CCD detector (Bruker, Karlsruhe, Germany) and a high-brilliance Iμs 3.0 microfocus anode (Ag radiation) (Incoatec, Geesthacht, Germany). The exposure time was 5 s per frame. Lorentz and polarization corrections, as well as an analytical absorption correction based on the crystal shape were applied to the reflection intensities, using the CrysAlis Pro package [23].

All high-pressure experiments were performed using the diamond anvil cells (DAC). Pressure was generated by means of four-screw-driven BX90 type DACs [24] equipped with Boehler-Almax [25] anvils (250 μm culet sizes). Rhenium gaskets were indented to about 25 μm of thickness. A 120 μm hole was drilled in the middle of the indentation. The gaskets were then placed between two diamonds to form a pressure chamber. Neon loaded at about 1.2 kbar [26] was used as a pressure-transmitting medium. Note that the neon might have a limitation on hydrostaticity at 15 GPA [27]. However, we see no indication of that in our experiment. In each loading, two δ-AlOOH single crystals with dimensions of ~0.02 × 0.02 × 0.01 mm^3 were put in DACs along with a ruby for pressure calibration [28]. Here, we report the data for the best crystal in each experiment.

Single crystal X-ray diffraction high-pressure experiments were performed at P02.2 at PETRA III and at ID15 at ESRF. At extreme conditions, the beamline P02.2 at PETRA III data were collected using a PerkinElmer flat panel detector and X-ray radiation with a wavelength of λ = 0.28995 Å and beam size of 2 μm^2. At the beam line ID15 at ESRF, data were acquired using the MAR555 detector and X-ray radiation with a wavelength of λ = 0.28874 Å and beam size of 2 μm^2. Diffraction data were collected at room temperature and the pressure was from 3 to 30 GPa with a step of 2–4 GPa. Each frame was measured for 0.5 s. Integration of the reflection intensities and absorption corrections were performed using the CrysAlisPro software [23]. Please note that the graphs of the unit cell parameters from the two experiments, while internally consistent, differ between themselves. We have kept both datasets and marked them on the plots as an indication for systematic errors. The estimates of the statistical errors on experimental parameters were obtained from the integration and refinement software, the errors on the pressure were assumed to be equal to 0.5 GPa.

All crystallographic data refinements were performed based on F^2 using the SHELX97 program package [29] in the WinGX System [30]. Due to the low completeness common for high-pressure experiments, hydrogen atoms could not be reliably identified from the different electron densities. The fitting of the equation of states were performed in program EOSFit7 [31].

3. Results and Discussion

Selected examples of the results of the structural refinement of δ-AlOOH at different pressures are presented in Table 1 (see also the CIF files provided in Supplementary Materials). For all data-points, we collected more than 100 reflections, which after integration in CrysAlis Pro gave R_{int} about 3% and refined to R1 better than 5% (Table 1). Remarkably, the high-pressure data allowed the comparable quality of the structural refinement as those obtained at ambient conditions, which gives evidence that the crystals were in a quasi-hydrostatic environment up to the highest pressures achieved.

Table 1. Crystallographic data for $P2_1nm$ (7.85 GPa) and *Pnnm* (10.19 GPa) phases of δ-AlOOH at room temperature.

Parameter	$P2_1nm$	$P2_1nm$	*Pnnm*	*Pnnm*
Facility		P02.2 PETRA III	P02.2 PETRA III	P02.2 PETRA III
Pressure (GPa)	ambient	7.85	10.19	29.35
Empirical formula	AlOOH	AlOOH	AlOOH	AlOOH
Formula weight (g/mol)	59.99	59.99	59.99	59.99
Wavelength (Å)	0.5608	0.2887	0.2887	0.2887
Crystal system	Orthorhombic	Orthorhombic	Orthorhombic	Orthorhombic
Space group	$P2_1nm$	$P2_1nm$	*Pnnm*	*Pnnm*
a (Å)	4.7202(8)	4.640(2)	4.6244(12)	4.5288(19)
b (Å)	4.2259(6)	4.13709(19)	4.1225(3)	4.0345(4)
c (Å)	2.8278(4)	2.8017(3)	2.79255(18)	2.7278(4)
V (Å^3)	56.406(15)	53.78(2)	53.237(15)	49.84(2)
Z	2	2	2	2
Calculated density (g/cm^3)	3.54	3.704	3.742	3.997
Crystal size (μm^3)	20 × 20 × 30	20 × 20 × 30	20 × 20 × 30	20 × 20 × 30
Theta range for data collection (deg)	4.0320 to 28.6530	3.568 to 18.223	3.580 to 18.287	3.663 to 17.658
Index range	−4 < h < 4 −6 < k < 6 −7 < l < 4	−5 < h < 3 −7 < k < 6 −5 < l < 4	−4 < h < 5 −7 < k < 6 −5 < l < 4	−4 < h < 5 −7 < k < 6 −4 < l < 4
Reflections used	644	284	310	108
Rint	0.026	0.045	0.031	0.035
Refinement method	Least squares on F2	Least squares on F2	Least squares on F2	Least squares on F2
Restraints/parameters	0/15	1/15	0/9	0/9
Goodness of fit on F2	1.065	1.284	1.088	1.088
Final R indices [I > 2σ(I)]	R1 = 0.0257	R1 = 0.0451	R1 = 0.0336	R1 = 0.0346
R indices (all data)	R1 = 0.0247; wR2 = 0.0658	R1 = 0.0446; wR2 = 0.1317	R1 = 0.0319; wR2 = 0.0778	R1 = 0.0351; wR2 = 0.1016
Largest diff. peak and hole (e/Å3)	0.59 and −0.37	0.92 and −0.74	0.45 and −0.78	0.58 and −0.76

The δ-AlOOH crystallizes in an orthorhombic structure (space group $P2_1nm$) and can be described in terms of a slightly distorted hexagonally close packed arrangement of O anions with Al cations occupying two-thirds of the octahedral sites (Figures 1 and 2). The AlO_6 octahedra are linked together by sharing edges and vertices to form infinite 2×1 channels parallel to the **b** axis with H atoms inside the channels. There are two independent oxygen sites: O1, at ambient conditions covalently bound to hydrogen (O-H bond), and O2, characterized by a weak H···O bond. In the selected octahedron, one can distinguish the O1a and O2a atoms in the axial position and two O1e and O2e atoms in the equatorial position. The octahedral $Al(O-H)_3$ $(O···H)_3$ moiety is highly distorted at ambient pressure, as seen in Figure 2, where the Al-O1 bonds are significantly longer than those of Al-O2.

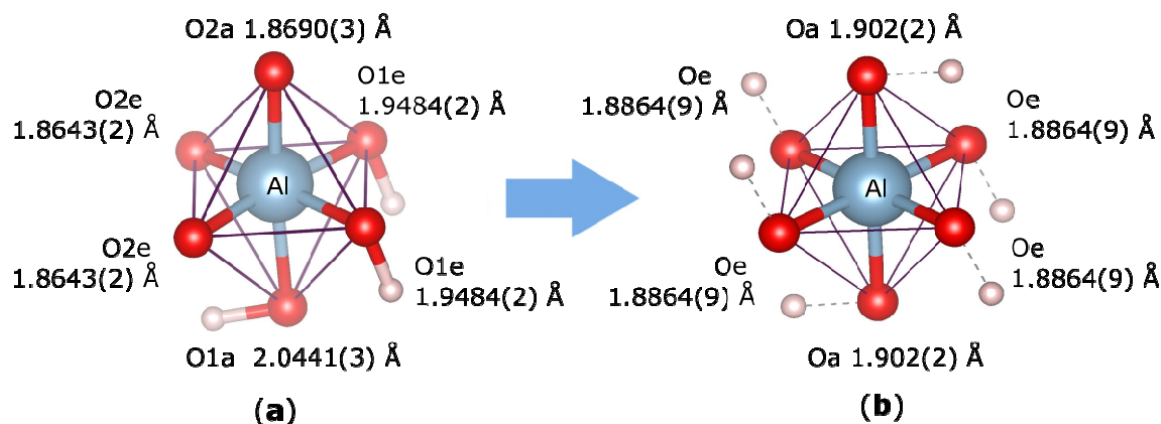**Figure 2.** AlO_6 octahedron at ambient pressure (**a**) and after transition at ~10.19 GPa (**b**).

A close examination of diffraction images shows that between 7.85 and 10.19 GPa certain changes occur (Figure 3). At 7.85, the reflection extinction conditions are consistent with the 2_1 screw axis along **a** (h00: h = 2n) and with the n-glide plane perpendicular to **b** (h0l, h + l = 2n). However, at 10.19 GPa, the new extinction rule becomes valid (*0kl*: k + l = 2n) (Figure 3b). This corresponds to the appearance of a new *n*-glide plane in the system and overall increase of the symmetry from $P2_1nm$ to *Pnnm* (Figure 1). Therefore, this confirms the structural phase transition between 7.85 and 10.19 GPa.

Unit cell parameters of δ-AlOOH at ambient conditions are a = 4.7202(8) Å, b = 4.2259(6) Å, c = 2.8278(4) Å, and V = 56.406(15) Å^3 (Table 1), in good agreement with literature data [9,13,15,32].

In total, X-ray diffraction data were collected at 16 different pressures (Table 2). The dependence of the unit cell volume of δ-AlOOH on a pressure up to 30 GPa is shown in Figure 4. The equation of states was fitted with the second order Birch-Murnaghan (BM2) equation for low-pressure and high-pressure data separately and gave the following results: K_0 = 142(8) GPa below the phase transition and K_0 = 216(5) GPa above the phase transition. Just for comparison with the literature, the third-order Birch-Murnaghan (BM3) equation of state was also fitted over the whole volume range, as presented in Table 3. Our results are in good agreement with the results of Suzuki [9] and Sano-Furukawa [11], while in stark discrepancy with the results of Vanpeteghem et al. [13]. The reason for the discrepancy with Vanpeteghem et al. [13] is not obvious and we only hypothesized that it may relate to the diffusion of He (employed as a pressure medium by Vanpeteghem et al.) into the bulk of δ-AlOOH.
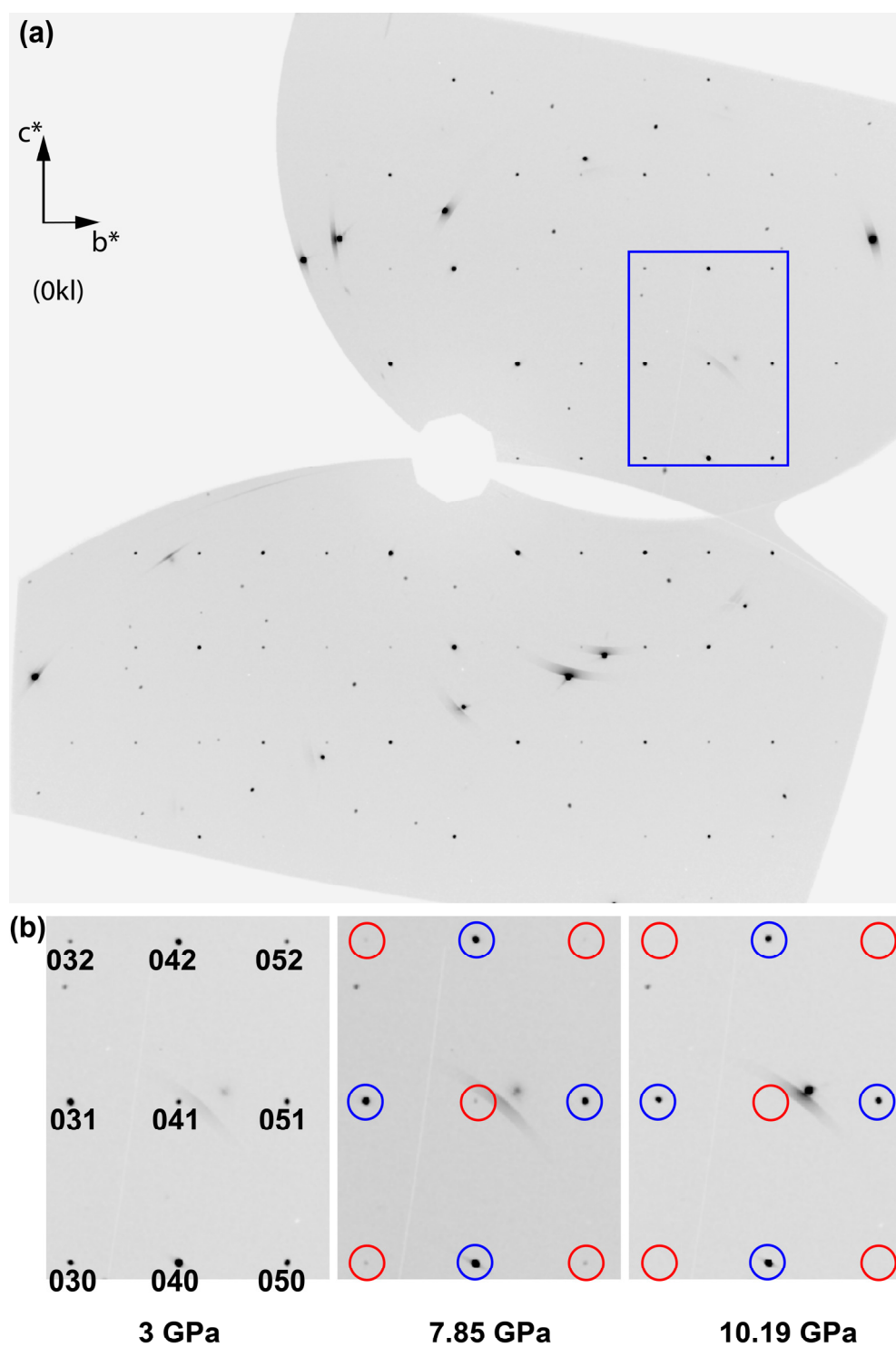
Figure 3. (**a**) Single crystal diffraction precession image of δ-AlOOH along the *0kl*. The blue square shows the area that was enlarged in Figure 3b. (**b**) The enlarged single crystal diffraction precession images of δ-AlOOH of the *0kl* section at different pressures. "***"—designate vectors of reciprocal lattice.

Table 2. Lattice parameters for δ-AlOOH at different pressure points.

| Experiment	Pressure, GPa	a, Å	b, Å	c, Å	V, Å3
in-house	ambient	4.7202(8)	4.2259(6)	2.8278(4)	56.406(15)
DESY	3.16	4.68246(12)	4.18746(17)	2.8197(8)	55.288(16)
ESRF	3.42	4.6824(3)	4.18642(15)	2.8196(3)	55.271(7)
DESY	5.27	4.6612(9)	4.1613(2)	2.81066(15)	54.518(12)
DESY	7.85	4.640(2)	4.13709(19)	2.8017(3)	53.78(2)
ESRF	8.74	4.6316(2)	4.12766(18)	2.79637(15)	53.460(4)
DESY	10.19	4.6244(12)	4.1225(3)	2.79255(18)	53.237(15)
ESRF	11.8	4.6127(2)	4.11221(14)	2.78493(14)	52.826(4)
DESY	12.75	4.6087(13)	4.1090(3)	2.7836(2)	52.713(16)
DESY	15.14	4.5977(13)	4.0958(3)	2.7744(2)	52.245(16)
ESRF	17.64	4.5787(5)	4.0854(2)	2.76353(11)	51.694(6)
DESY	18.25	4.5809(15)	4.0814(3)	2.7639(3)	51.675(18)
DESY	21.24	4.5672(13)	4.0680(3)	2.7546(2)	51.179(16)
ESRF	22.4	4.5493(7)	4.0646(4)	2.74858(17)	50.824(10)
DESY	25.03	4.545(2)	4.0524(4)	2.7417(4)	50.50(3)
DESY	29.35	4.5288(19)	4.0345(4)	2.7278(4)	49.84(2)
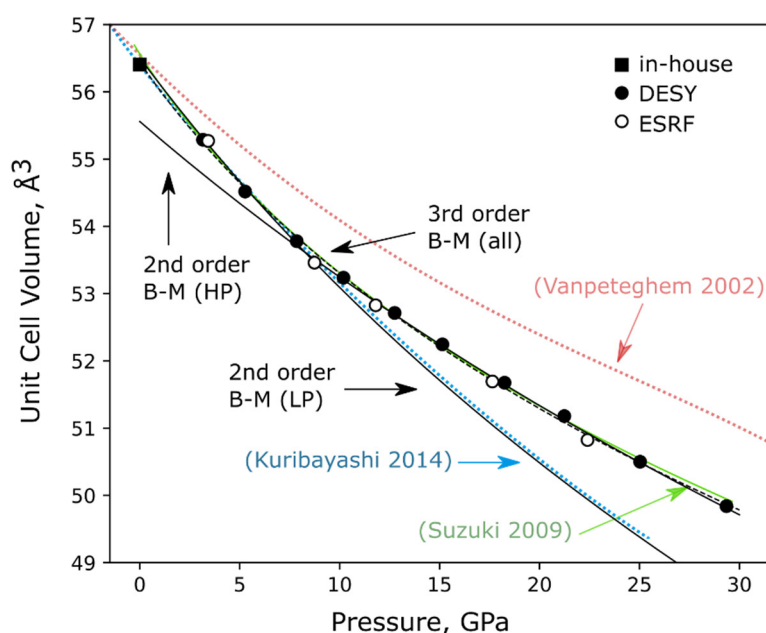
Figure 4. Compressibility data for δ-AlOOH in this study (black) compared with the trend of literature data [10] (green), [21] (blue), and [9] (red). Error bars are smaller than the marker sizes.

Table 3. Refined parameters for the δ-AlOOH equation of state.

Fitting Model	V_0, Å^3	K_0, GPa	K'
Third order BM, full range	56.43(9)	132(8)	10(1)
Second order BM, low pressure	56.51(8)	142(5)	4(fixed)
Second order BM, high pressure	55.56(8)	216(5)	4(fixed)

The pressure dependence of the unit cell parameters of δ-AlOOH is shown in Figure 5. As can be seen, below the phase transition the **b** and **a** axes are more susceptible than the **c** axis since the soft hydrogen bonds lie in the a-b plane. Above the phase transition, the compressibility in all axes becomes comparable. As seen in Figure 6a, this change in compressibility is defined solely by the hydrogen, while all other bonds decrease in pressure monotonically and almost linearly (Figure 6a,b).
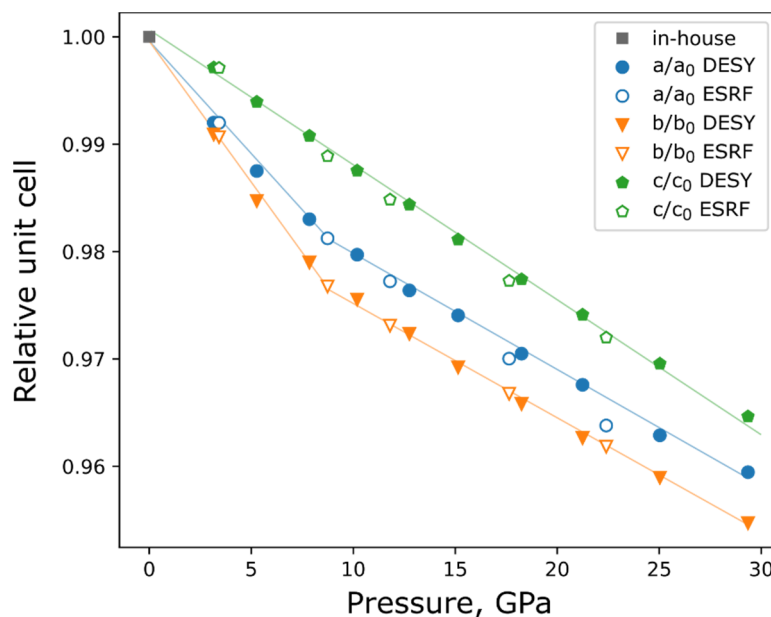
Figure 5. Variation of relative lattice parameters of δ-AlOOH with pressure. Lines are guides to the eye and error bars are smaller than the marker sizes.
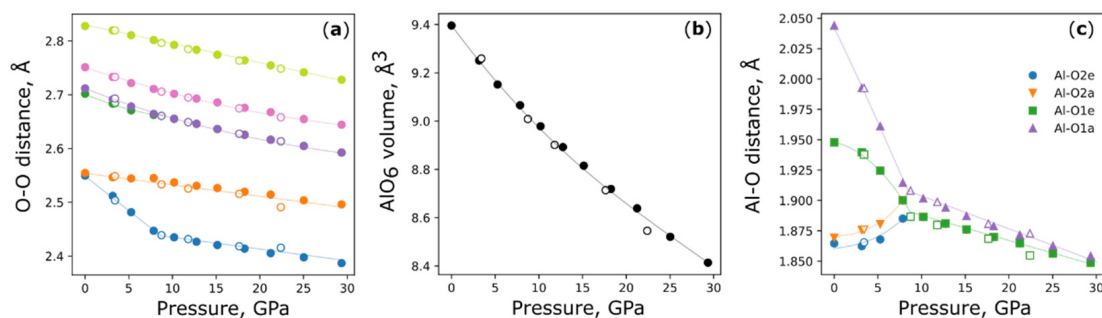
Figure 6. (**a**) Evolution of the shortest oxygen-oxygen distances with pressure, blue is hydrogen bond, other curves are O-O distances within the AlO_6 octahedron; (**b**) pressure-dependent evolution of the AlO_6 octahedron volume; (**c**) evolution of Al-O bonds within the AlO_6 polyhedra (see Figure 2 for atoms assignment). Lines are guides for the eye and error bars are smaller than the marker sizes.

It is interesting to note that we could not observe any structural change around 16 GPa, which was estimated by neutron diffractions as the pressure where the hydrogen bond changes from a disordered to single-well symmetric type [12]. X-ray data are not directly sensitive to the hydrogen atoms. However, the atomic parameters of other atoms indirectly indicate any significant changes. For instance, the approach of the phase transition around 10 GPa is clearly visible in the asymmetry of Al position within the oxygen octahedron (Figure 6c). As for the region of 16 GPa, neither the O-H-O compressibility (Figure 6a) nor other structural parameters indicate any change within the observed accuracy. Our observation is similar to that of IR spectroscopy, which also did not indicate any anomalies at 16 GPa [33]. More intensive diffraction and modelling studies will be required to understand the stiffening in δ-AlOOH, which is defined by crystallographic symmetry rather than the nature of hydrogen bond.

4. Conclusions

We obtained an accurate equation of the state of δ-AlOOH, up to 30 GPa, from the compression of single crystals in a quasi-hydrostatic pressure medium. The evolution of the structure of δ-AlOOH with pressure was characterized in detail and revealed a phase transition approximately above 10 GPa, associated with an increase of the bulk modulus from 142(5) to 216(5) GPa. The phase

transition is caused by the increase in the hydrogen bond symmetry caused by a disorder. We could not identify any structural difference at 16 GPa, which was suggested as the pressure of hydrogen bond symmetrization. This makes δ-AlOOH an unusual material, in which hydrogen bond stiffening is governed by crystallographic symmetry.

References

1. Panero, W.R.; Caracas, R. Stability of phase H in the $MgSiO_4H_2$–AlOOH–SiO_2 system. *Earth Planet. Sci. Lett.* **2017**, *463*, 171–177. [CrossRef]

2. Nishi, M.; Irifune, T.; Tsuchiya, J.; Tange, Y.; Nishihara, Y.; Fujino, K.; Higo, Y. Stability of hydrous silicate at high pressures and water transport to the deep lower mantle. *Nat. Geosci.* **2014**, *7*, 224–227. [CrossRef]

3. Wirth, R.; Vollmer, C.; Brenker, F.; Matsyuk, S.; Kaminsky, F. Inclusions of nanocrystalline hydrous aluminium silicate "Phase Egg" in superdeep diamonds from Juina (Mato Grosso State, Brazil). *Earth Planet. Sci. Lett.* **2007**, *259*, 384–399. [CrossRef]

4. Ono, S. Stability limits of hydrous minerals in sediment and mid-ocean ridge basalt compositions: Implications for water transport in subduction zones. *J. Geophys. Res. Space Phys.* **1998**, *103*, 18253–18267. [CrossRef]

5. Sano, A.; Ohtani, E.; Kubo, T.; Funakoshi, K.-I. In situ X-ray observation of decomposition of hydrous aluminum silicate $AlSiO_3OH$ and aluminum oxide hydroxide d-AlOOH at high pressure and temperature. *J. Phys. Chem. Solids* **2004**, *65*, 1547–1554. [CrossRef]

6. Sano, A.; Ohtani, E.; Kondo, T.; Hirao, N.; Sakai, T.; Sata, N.; Ohishi, Y.; Kikegawa, T. Aluminous hydrous mineralδ-AlOOH as a carrier of hydrogen into the core-mantle boundary. *Geophys. Res. Lett.* **2008**, *35*, 1–5. [CrossRef]

7. Yoshino, T.; Baker, E.; Duffey, K. Fate of water in subducted hydrous sediments deduced from stability fields of FeOOH and AlOOH up to 20 GPa. *Phys. Earth Planet. Inter.* **2019**, *294*, 106295. [CrossRef]

8. Suzuki, A.; Ohtani, E.; Kamada, T. A new hydrous phase δ-AlOOH synthesized at 21 GPa and 1000 °C. *Phys. Chem. Miner.* **2000**, *27*, 689–693. [CrossRef]

9. Vanpeteghem, C.B.; Ohtani, E.; Kondo, T. Equation of state of the hydrous phase δ-AlOOH at room temperature up to 22.5 GPa. *Geophys. Res. Lett.* **2002**, *29*, 1119. [CrossRef]

10. Suzuki, A. Compressibility of the high-pressure polymorph of AlOOH to 17 GPa. *Miner. Mag.* **2009**, *73*, 479–485. [CrossRef]

11. Sano, A.; Kagi, H.; Nagai, T.; Nakano, S.; Fukura, S.; Ushijima, D.; Iizuka, R.; Ohtani, E.; Yagi, T. Change in compressibility of -AlOOH and -AlOOD at high pressure: A study of isotope effect and hydrogen-bond symmetrization. *Am. Miner.* **2009**, *94*, 1255–1261. [CrossRef]

12. Sano-Furukawa, A.; Hattori, T.; Komatsu, K.; Kagi, H.; Nagai, T.; Molaison, J.J.; Dos Santos, A.M.; Tulk, C.A. Direct observation of symmetrization of hydrogen bond in δ-AlOOH under mantle conditions using neutron diffraction. *Sci. Rep.* **2018**, *8*, 15520. [CrossRef] [PubMed]

13. Terasaki, H.; Ohtani, E.; Sakai, T.; Kamada, S.; Asanuma, H.; Shibazaki, Y.; Hirao, N.; Sata, N.; Ohishi, Y.; Sakamaki, T.; et al. Stability of Fe–Ni hydride after the reaction between Fe–Ni alloy and hydrous phase (δ-AlOOH) up to 1.2Mbar: Possibility of H contribution to the core density deficit. *Phys. Earth Planet. Inter.* **2012**, *194*, 18–24. [CrossRef]

14. Tsuchiya, J.; Tsuchiya, T. First-principles prediction of a high-pressure hydrous phase of AlOOH. *Phys. Rev. B* **2011**, *83*, 2–5. [CrossRef]

15. Zhong, X.; Hermann, A.; Wang, Y.; Ma, Y. Monoclinic high-pressure polymorph of AlOOH predicted from first principles. *Phys. Rev. B* **2016**, *94*, 224110. [CrossRef]

16. Piet, H.; Leinenweber, K.D.; Tappan, J.; Greenberg, E.; Prakapenka, V.B.; Buseck, P.R.; Shim, S.-H. Dehydration of δ-AlOOH in Earth's Deep Lower Mantle. *Minerals* **2020**, *10*, 384. [CrossRef]

17. Nishi, M.; Kuwayama, Y.; Tsuchiya, J. New aluminium hydroxide at multimegabar pressures: Implications for water reservoirs in deep planetary interiors. *Icarus* **2020**, *338*, 113539. [CrossRef]

18. Tsuchiya, J.; Tsuchiya, T. Elastic properties of δ-AlOOH under pressure: First principles investigation. *Phys. Earth Planet. Inter.* **2009**, *174*, 122–127. [CrossRef]

19. Mashino, I.; Murakami, M.; Ohtani, E. Sound velocities of δ-AlOOH up to core-mantle boundary pressures with implications for the seismic anomalies in the deep mantle. *J. Geophys. Res. Solid Earth* **2016**, *121*, 595–609. [CrossRef]

20. Ohtani, E.; Litasov, K.; Suzuki, A.; Kondo, T. Stability field of new hydrous phase, δ-AlOOH, with implications for water transport into the deep mantle. *Geophys. Res. Lett.* **2001**, *28*, 3991–3993. [CrossRef]

21. Kuribayashi, T.; Sano, A.; Nagase, T. Observation of pressure-induced phase transition of δ-AlOOH by using single-crystal synchrotron X-ray diffraction method. *Phys. Chem. Miner.* **2013**, *41*, 303–312. [CrossRef]

22. Bronstein, Y.; Depondt, P.; Finocchi, F. Thermal and nuclear quantum effects in the hydrogen bond dynamical symmetrization phase transition of δ-AlOOH. *Eur. J. Miner.* **2017**, *29*, 385–395. [CrossRef]

23. *CrysAlis Pro*; Rigaku Oxford Diffraction Ltd.: Yarnton/Oxfordshire, UK, 2017; Available online: https://www.rigaku.com/products/smc/crysalis (accessed on 23 November 2020).

24. Kantor, I.; Prakapenka, V.; Kantor, A.; Dera, P.; Kurnosov, A.; Sinogeikin, S.; Dubrovinskaia, N.; Dubrovinsky, L. BX90: A new diamond anvil cell design for X-ray diffraction and optical measurements. *Rev. Sci. Instrum.* **2012**, *83*, 125102. [CrossRef] [PubMed]

25. Boehler, R. New diamond cell for single-crystal X-ray diffraction. *Rev. Sci. Instrum.* **2006**, *77*, 115103. [CrossRef]

26. Kurnosov, A.; Kantor, I.; Ballaran, T.B.; Lindhardt, S.; Dubrovinsky, L.S.; Kuznetsov, A.; Zehnder, B.H. A novel gas-loading system for mechanically closing of various types of diamond anvil cells. *Rev. Sci. Instrum.* **2008**, *79*, 45110. [CrossRef] [PubMed]

27. Klotz, S.; Chervin, J.-C.; Munsch, P.; Le Marchand, G. Hydrostatic limits of 11 pressure transmitting media. *J. Phys. D Appl. Phys.* **2009**, *42*, 075413. [CrossRef]

28. Mao, H.K.; Xu, J.; Bell, P.M. Calibration of the ruby pressure gauge to 800 kbar under quasi-hydrostatic conditions. *J. Geophys. Res. Space Phys.* **1986**, *91*, 4673–4676. [CrossRef]

29. Sheldrick, G.M. A short history of SHELX. *Acta Crystallogr. Sect. A Found. Crystallogr.* **2008**, *64*, 112–122. [CrossRef]

30. Farrugia, L.J. WinGXsuite for small-molecule single-crystal crystallography. *J. Appl. Crystallogr.* **1999**, *32*, 837–838. [CrossRef]

31. Gonzalez-Platas, J.; Alvaro, M.; Nestola, F.; Angel, R. EosFit7-GUI: A new graphical user interface for equation of state calculations, analyses and teaching. *J. Appl. Crystallogr.* **2016**, *49*, 1377–1382. [CrossRef]

32. Komatsu, K.; Kuribayashi, T.; Sano, A.; Ohtani, E.; Kudoh, Y. Redetermination of the high-pressure modification of AlOOH from single-crystal synchrotron data. *Acta Crystallogr. Sect. E Struct. Rep. Online* **2006**, *62*, i216–i218. [CrossRef]

33. Kagi, H.; Ushijima, D.; Sano, A.; Komatsu, K.; Iizuka, R.; Nagai, T.; Nakano, S. Infrared absorption spectra of δ-AlOOH and its deuteride at high pressure and implication to pressure response of the hydrogen bonds. *J. Phys. Conf. Ser.* **2010**, *215*, 012052. [CrossRef]